Study of Rotary-Linear Ultrasonic Motor Output Shafts

Kanada, Ayato
Toyohashi University of Technology

Mashimo, Tomoaki
Toyohashi University of Technology

Terashima, Kazuhiko
Toyohashi University of Technology

出版情報：International Journal of Automation Technology. 10 (4), pp.549-556, 2016-07-05. 富士技術出版株式会社
バージョン：

https://doi.org/10.20965/ijat.2016.p0549

Paper:

Study of Rotary-Linear Ultrasonic Motor Output Shafts

Ayato Kanada†, Tomoaki Mashimo, and Kazuhiko Terashima

Toyohashi University of Technology
1-1 Hibarigaoka, Tempaku-cho, Toyohashi, Aichi 441-8580, Japan
†Corresponding author, E-mail: kanada@syscon.me.tut.ac.jp
[Received January 5, 2016; accepted May 6, 2016]

We propose output shafts with a preload generation mechanism to improve the output torque and thrust force of the rotary-linear ultrasonic motor. The stator is comprised of a single metallic cube with a through-hole, and the output shafts are inserted into the hole to generate motion in both its circumferential and axial directions arbitrarily. In this paper, two design concepts for optimizing the preload using the output shafts are examined. The first involves a cylinder shaft with micron-order accuracy diameter realization. The cylinder shaft makes contact with the entire inner surface of the stator and generates a preload between the stator and shaft. The second concept employs a spring shaft having a slightly larger diameter than the stator hole, which expands in the radial direction and generates the preload. Experiments show that these design concepts improve the output torque and thrust force.

Keywords: actuator, piezoelectricity, multi-DOF, preload mechanism

1. Introduction

Both rotational and translational motions are required in a wide range of industrial applications, such as positioning stages. For example, in product assembly lines, mechanical components are approached using translation and precisely attached to products using rotation. The most basic concepts for the construction of such automated devices with multiple degrees of freedom (multi-DOF) involve the use of several one-DOF actuators and transmissions. Rotary-linear actuators that drive an output shaft in its circumferential and axial directions based on a variety of driving principles have been proposed. The electro-magnetic force, the most commonly used force in actuator design, has been used for rotary-linear motors for approximately 30 years [1, 2]. One practical example is a pneumatic rotary-linear actuator used for positioning in industrial devices [3].

The piezoelectric effect is an attractive principle as regards the generation of both rotary and linear motion. Many researchers have developed a rotary-linear actuating system using two or three piezoelectric actuators [4–7]. However, these mechanisms are large and complex, because they employ a large number of components. Another approach towards the use of piezoelectric effects for the generation of rotary and linear motion is the use of the smooth impact drive method (SIDM) [8]. The SIDM-based rotary-linear actuator is relatively simple; however, its torque and force do not reach the required practical level.

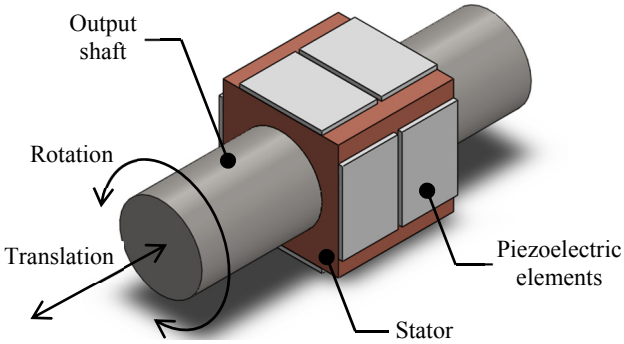

Fig. 1. Schematic of rotary-linear ultrasonic motor.

We have constructed a rotary-linear piezoelectric ultrasonic motor comprised of a cubic stator and an output shaft [9, 10]. As shown in **Fig. 1**, the stator is a single metallic cube with a through-hole. An output shaft is inserted into the through-hole; the shaft spins in the through-hole circumferential direction and moves in its axial direction. One of the important advantages of the proposed motor is the simplicity of the stator, which can render fabrication easy and inexpensive. In our previous paper, the driving principle for rotary and linear motion generation was verified for this motor; however, the output torque and thrust force were still under development [9].

The goal of this paper is to improve the torque and thrust force of the rotary-linear ultrasonic motor, using two design concepts concerning the output shaft and preload. The first concept is the use of a cylinder shaft with micron-order accuracy in its diameter measurement. When the cylinder shaft is inserted into the stator hole with no clearance between the stator and shaft, it makes contact with the entire inner surface of the stator and generates a preload. The other design concept involves a spring shaft having a slightly larger diameter than the stator hole diameter. When the spring shaft is inserted into the stator, it expands in the radial direction and generates a preload. These output shafts can provide an optimal preload to the stator and generate a higher motor torque and thrust force.

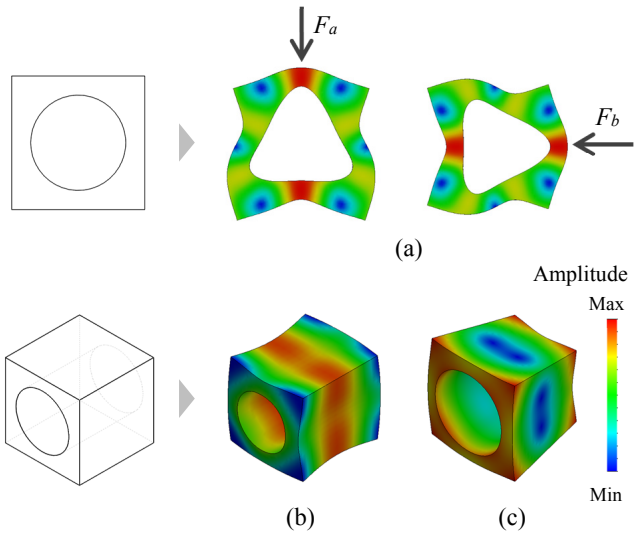

Fig. 2. Vibration modes for rotation and translation: (a) R3 mode, (b) T1 mode and (c) T2 mode.

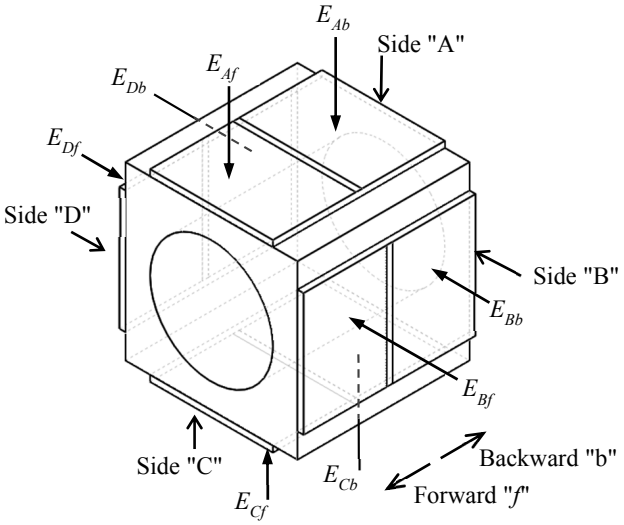

Fig. 3. Schematic of stator and applied voltages.

2. Driving Principle and Modal Analysis

The stator of the rotary-linear ultrasonic motor excites individual vibration modes for rotary and linear motions as the driving principle [9]. The rotation is based on a vibration mode that excites three waves along the circumference of the through-hole (R3 mode) shown in **Fig. 2(a)**. When a periodic force F_a acts on the top surface of the stator by piezoelectric effect, a standing wave R3 mode is generated. When the other periodic force F_b acts on the next surface with 90 degrees, another R3 mode is excited. By generating these two R3 modes with the temporal phase difference of $\pi/2$ (one-quarter of a cycle) simultaneously, the travelling wave is produced on the inner surface of the through-hole. While producing the traveling wave, elliptical motion is generated, and it moves the output shaft in the circumferential direction. This driving principle of the rotation is the same as that of the traveling type ultrasonic motor [11], although it appears different design.

The linear motion is generated by coupling the first extension mode (T1 mode) and the second extension mode (T2 mode) of the stator shown in **Figs. 2(b)** and **(c)**, respectively. T1 mode is symmetry and the T2 mode is asymmetry with respect to the axial direction. When the stator design is cubic, the natural frequency of T1 mode and T2 mode are accorded. This fact has been verified by vibration analyses in existing literature [9, 12]. Giving the temporal phase difference $\pi/2$ between Tl mode and T2 mode, the inner surface of the stator generates an elliptical motion that moves the output shaft in the axial direction. Such driving principle for the linear motion is well-known in linear ultrasonic motors [13, 14] and multi-degree of freedom ultrasonic motors [15, 16]. In these motors, combination of the first extension mode and the second bending mode is used as their driving principle.

Modal analysis using finite element methods (FEM) clarifies mode shapes and natural frequencies of the stator. The material characteristics of the stator used in FEM model are the same as those of phosphor bronze. The stator shape is a single metallic cube with a side length of 14 mm and a through-hole of 10 mm in diameter. The modal analysis shows the mode shape of R3, T1, and T2 modes as shown in **Fig. 2**. The resultant R3 mode is excited at approximately 66.7 kHz. The resultant T1 and T2 modes are observed at 78.0 kHz and 77.5 kHz, respectively.

3. Stator Characteristics

3.1. Stator Schematic

A schematic of the rotary-linear ultrasonic motor stator is shown in **Fig. 3**. Four plate piezoelectric elements (Material: HC-51GS; Honda Electronics Co., Japan) are bonded on the four sides of a cube composed of phosphor bronze. Each piezoelectric element has two silver electrodes with positive polarization on one side. In total, there are eight electrodes on the outside of the stator. On the other side, a negatively polarized silver electrode conducts electricity to the metallic body and ground reference of the power supply devices. Voltages are applied by eight wires, which are each connected to the eight electrodes, as shown in **Fig. 3**. The four sides of the stator are labeled "A"−"D" in a clockwise direction, and the forward and backward axial directions are labeled "f" and "b," respectively. The voltages applied to all silver electrodes of the eight piezoelectric elements are labeled as "E_{Af}," "E_{Ab}" to "E_{Db}," "E_{Df}." To generate rotation, four voltage types with a phase shift of $\pi/2$ are applied:

$$E_{Af} = E_{Ab} = A_E \sin(2\pi f_E t), \quad (1)$$
$$E_{Bf} = E_{Bb} = A_E \sin(2\pi f_E t + \pi/2), \quad (2)$$
$$E_{Cf} = E_{Cb} = A_E \sin(2\pi f_E t + \pi), \quad (3)$$
$$E_{Df} = E_{Db} = A_E \sin(2\pi f_E t + 3\pi/2), \quad (4)$$

where A_E is the amplitude and f_E is the frequency of the applied voltages. When f_E is in the vicinity of the natu-

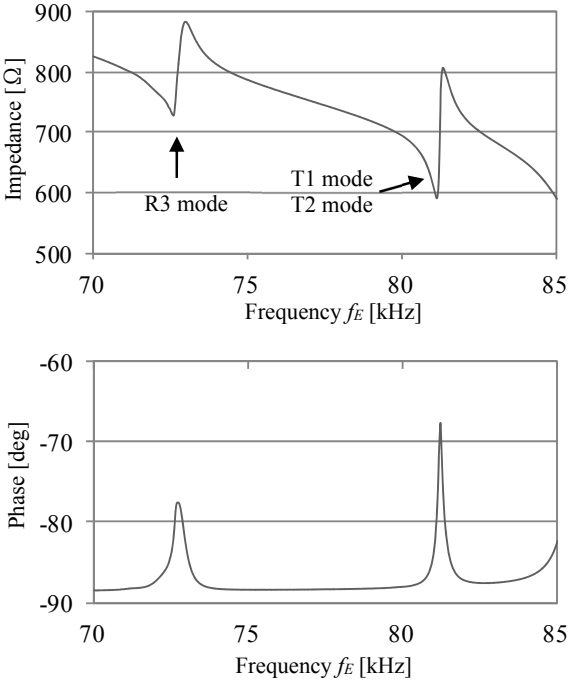

Fig. 4. Resonant frequency of R3, T1, and T2 modes.

ral frequency of R3 mode, the vibration amplitude is enhanced, resulting in the production of a traveling wave with a large vibration amplitude.

To generate linear motion, two kinds of voltages with phase of $\pi/2$ are applied:

$$E_{Af} = E_{Bf} = E_{Cf} = E_{Df} = A_E \sin(2\pi f_E t), \quad \ldots \quad (5)$$

$$E_{Ab} = E_{Bb} = E_{Cb} = E_{Db} = A_E \sin(2\pi f_E t + \pi/2), \quad (6)$$

where f_E is set near the natural frequency that excites the T1 and T2 modes.

The voltages to be applied to the stator are generated by a multi-channels function generator (WF1974; NF Corp., Japan) and amplified by high-frequency amplifiers (HSA4052; NF Corp., Japan).

3.2. Impedance Analysis

The resonant frequency of the prototype stator can be determined using an impedance analyzer (IM3570; Hioki E. E. Co., Japan). A wire is soldered to a piezoelectric element electrode and the ground wire from the metallic cube is connected to the impedance analyzer. The bottom of the stator is fixed with a flexible adhesive. **Fig. 4** shows the frequency characteristics of the stator impedance and phase. Steep changes in the impedance are observed at the frequency close to the frequency estimated as the R3, T1 and T2 modes. The resonant frequency of R3 mode is shown at approximately 73 kHz and T1 and T2 modes at approximately 81 kHz are shown. These frequencies are slightly higher than the estimated frequency by the FEM modal analysis. This discrepancy is due to the stator being fixed to a test bench, which increases the resonant frequencies.

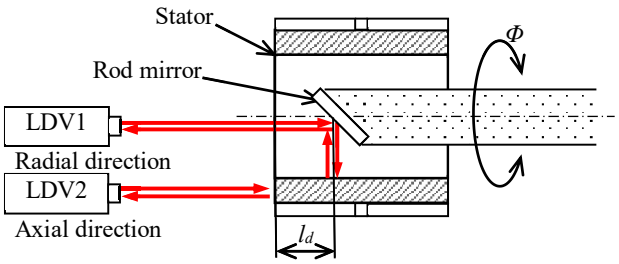

Fig. 5. Schematic diagram of vibration measurement using laser Doppler vibrometer (LDV).

3.3. Vibration Amplitude Measurement

The shape of the vibration modes can be clarified by measuring vibration amplitude. A laser Doppler vibrometer (LDV; NLV2500-5; Polytec, Germany), which outputs the vibration velocity of a point, is used for the measurement. By integrating the vibration velocity, we can obtain the vibration amplitude. Two LDVs, LDV1 and LDV2, are installed to measure the inner surface and the end of the stator, respectively, as shown in **Fig. 5**. The laser from LDV1 is aligned with the axis of the stator hole. A rod mirror located in the stator hole reflects the laser orthogonally to the inner surface of the through-hole. This reflection facilitates measurement of the radial vibration velocity. To define the mirror position, we denote Φ the angle of the mirror and l_d as the distance from the end of the stator to the center of the mirror. The other point that LDV2 measures is close to the stator hole at the end of metallic cube. The axial vibration amplitude of the stator is measured. By using these laser Doppler vibrometers and manipulating the rod mirror, the mode shapes and their vibration amplitudes are clarified.

The vibration amplitude of the R3 mode is measured by rotating the mirror in the direction of Φ. The gravity direction of the stator is defined as $\Phi = 0°$. To focus on a single R3 mode, the voltages expressed in Eqs. (1) and (3) are applied ($A_E = 120$ V_{p-p} and $f_E = 72.2$ kHz) and the voltages in Eqs. (2) and (4) are turned off. **Fig. 6(a)** shows the vibration amplitude inside the through-hole of the stator measured by LDV1 when rotating the mirror. The result shows the generation of three waves, in which the positive and negative are determined by the phase. The peak vibration amplitude of approximately 0.2 μm is obtained at the antinode of R3 mode. In fixing the angle Φ, radial vibration amplitude becomes roughly constant regardless of the direction of l_d. During the vibration of R3 mode, the vibration amplitude of the stator edge measured by LDV2 is approximately 0.013 μm.

The vibration amplitude of the stator excited by the T1 and T2 modes is measured by displacing the mirror in the direction of l_d. The voltages in Eqs. (5) and (6) are applied ($A_E = 120$ V_{p-p} and $f_E = 81.0$ kHz) in order to observe the vibration amplitude. **Fig. 6(b)** shows the vibration amplitude measured by LDV1 when the mirror is moved. The resultant vibration amplitude increases at both stator ends and decreases at the center, where the T2-mode node is located. The stator generates a peak vibration ampli-

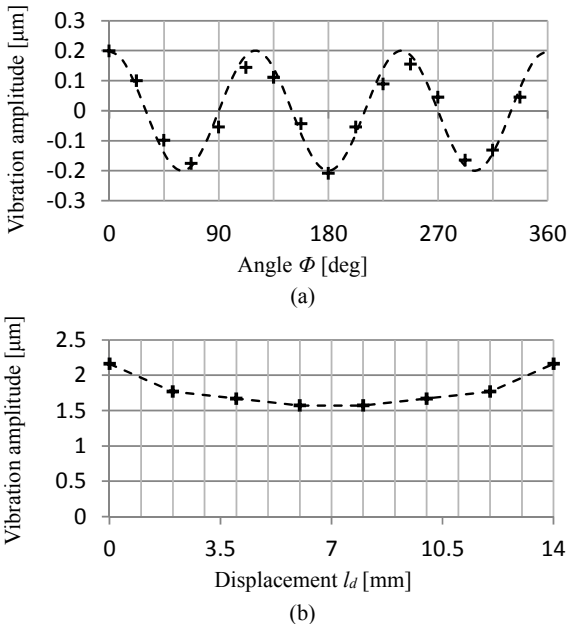

Fig. 6. Vibration amplitude of (a) R3 and (b) T1 and T2 modes.

tude of approximately 2.16 μm. The vibration amplitude measured by LDV2 is approximately 1.57 μm, which is roughly equal to the amplitude of the center. Compared to the peak amplitude of the R3 mode, the amplitude of T1 and T2 modes is more than ten times larger than the R3 mode.

4. Output Shafts and Preload Mechanisms

4.1. Proposal of Two Output Shafts

We propose two output shafts with a preload generation mechanism to solve this problem by: (i) adjusting clearance between a cylinder shaft and the stator hole and (ii) reducing a spring shaft to the stator diameter.

Figure 7(a) shows a preload method using the cylinder shaft. The cylinder shaft made of carbon steel has a weight of approximately 30.8 g; this weight becomes the preload between the stator and the shaft. To evaluate the contact between the cylinder shaft and the stator hole, let us denote dc the diameter of the cylinder shaft. When the cylinder diameter is smaller than the stator hole diameter ($d_c < D$), the shaft contacts with only the bottom of the through-hole by gravity. When the cylinder diameter is equal to the stator diameter ($d_c = D$), the outer surface of the shaft contacts the whole inner surface of the stator, and this contact condition is ideal for both rotation and linear motion. When the cylinder diameter is larger than the stator diameter ($d_c > D$), the friction force between the stator and the shaft increases and prevents the motor motions.

Figure 7(b) shows the other preload method using the spring shaft, which is the same one as a closed coil spring. The spring shaft is composed of stainless steel and has a diameter of d_s, weight of approximately 3 g, length of 30 mm, and a wire-diameter of 0.5 mm. When a moment is applied to the both ends of the spring shaft around the

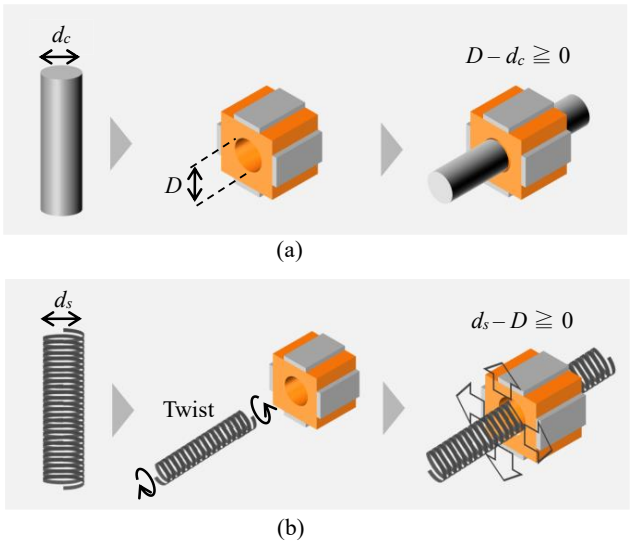

Fig. 7. Preload methods using (a) cylinder shaft and (b) spring shaft.

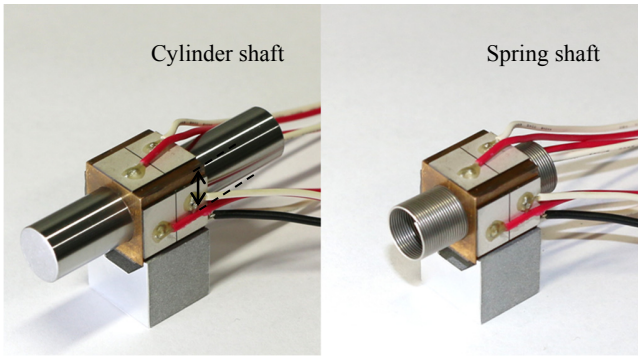

Fig. 8. Prototype motors with (a) cylinder shaft and (b) spring shaft.

axial direction, the spring shaft is twisted and its diameter decreases. While the spring shaft diameter is smaller than the stator hole diameter by twisting, the shaft is inserted to the stator. Then when the applied moment is removed, the outer diameter of the shaft expands to make even contact with the inner circumferential surface of the stator. This is an ideal condition, because the preload acts between the shaft and the stator without clearance. This preload can be optimized by choosing the spring shaft diameter: that is, the preload increases for larger spring diameters. Similar to the cylinder shaft, if the preload is too large, the friction force prevents the motor motion. **Figs. 8(a)** and **(b)** show the prototype motor with the cylinder shaft and the spring shaft, respectively.

4.2. Impedance Analysis

We examine how the impedance characteristics of the motor behave when the cylinder and the spring shafts are inserted into the stator. The f_R and f_T behavior is clarified by the impedance analyzer.

Figures 9(a) and **(b)** show the behavior of the resonant frequencies f_R and f_T, respectively, in changing the

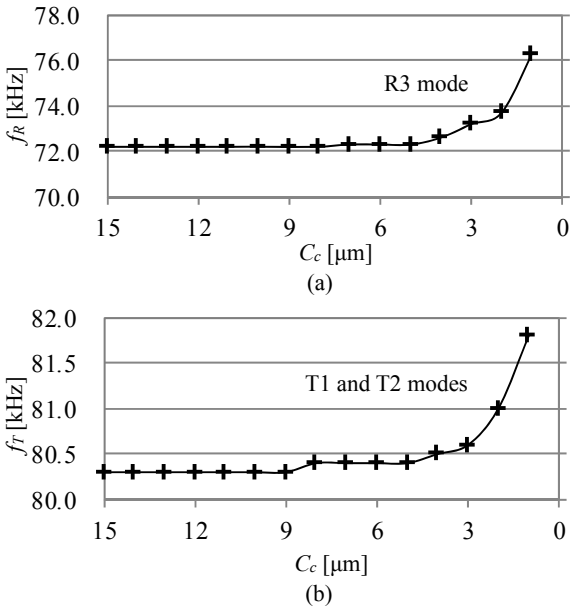

Fig. 9. Resonant frequencies for various cylinder shaft diameters: (a) R3 mode and (b) T1 and T2 modes (C_c: Clearance between stator and cylinder shafts, f_R: Resonant frequency of R3 mode, f_T: Resonant frequency of T1 and T2 modes).

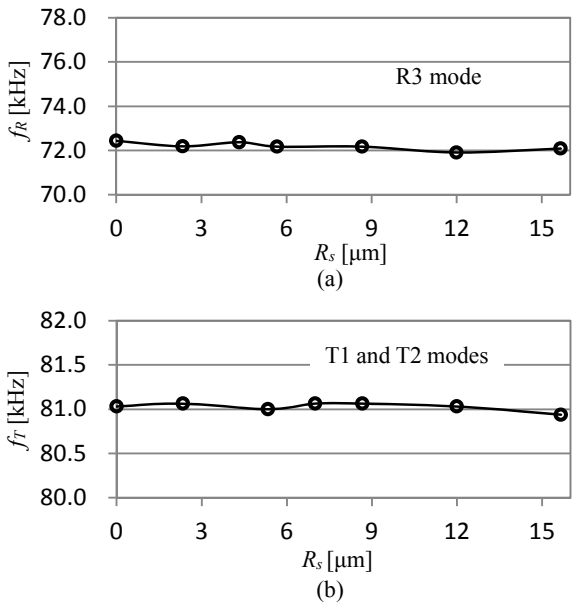

Fig. 10. Resonant frequencies for various spring shaft diameter: (a) R3 mode and (b) T1 and T2 modes (R_s: Reduction value of the spring shaft diameter, f_R: Resonant frequency of R3 mode, f_T: Resonant frequency of T1 and T2 modes).

cylinder shafts diameter with 1 μm accuracy. Note that several cylinder shafts were prepared for experiments as the output shaft. When the dimeter of the cylinder shaft is smaller than that of the stator hole, the shaft can be inserted to the stator hole smoothly. The clearance between the stator and the shaft decreases as the shaft diameter increases. When the shaft diameter is accorded with the stator hole, inserting the shaft into the hole needs a strong force. We determine this case as zero clearance. For evaluation of the cylinder shaft, we define clearance between the stator and the cylinder shafts C_c ($= D - d_c$) as the subtraction of the cylinder diameter from the stator diameter. When the clearance C_c is smaller than 4 μm, the both resonant frequencies sharply increase. This reveals that the outer diameter of the shaft contacts the inner circumferential surface of the stator without clearance. These resonant frequencies peak at $C_c = 1$ μm.

Figures 10(a) and **(b)** show the shift of the resonant frequencies in changing the spring shaft diameter, which is measured by a micrometer. The spring shaft is twisted to be inserted to the stator (**Fig. 7(b)**). The shaft diameter possible to be inserted without twisting is determined as zero clearance. This determination of the spring shaft clearance differs from that of the cylinder shaft. We define a reduction value of the spring diameter R_s ($= d_s - D$) as the subtraction of the stator diameter from the spring diameter. Also, R_s is an amount of shrinkage in spring shaft of the radial direction. The resonance frequency stays constant regardless of the reduction value R_s. This is because the spring shaft is hollow and its mass is very small, unlike the solid cylinder shaft.

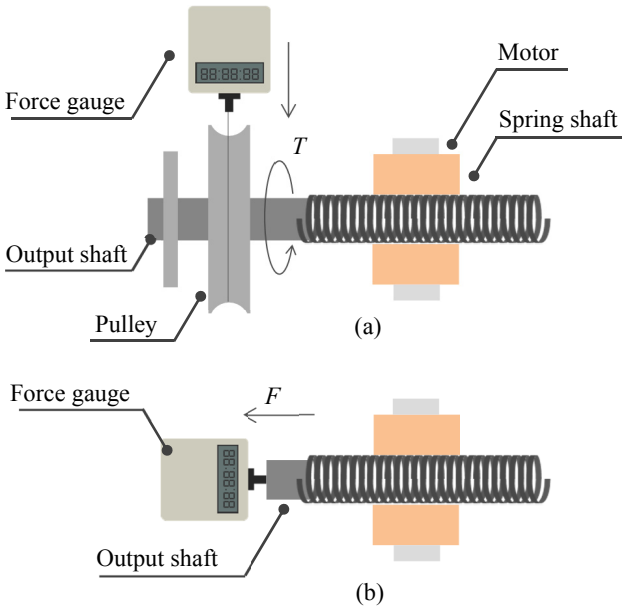

Fig. 11. Experimental setup for measuring (a) torque and (b) thrust force.

4.3. Torque and Thrust Force

We next demonstrate the manner in which Cc and Rs affect the torque and thrust force of the rotary-linear ultrasonic motor. **Fig. 11** shows the experimental setup for measuring the torque and thrust force. The torque and thrust force are statically measured by a force gauge (ZP-20N; Imada Co., Japan). In **Fig. 11(a)**, an output shaft is attached to the spring shaft, and its torque is measured by the force gauge via a pulley. In **Fig. 11(b)**, the output shaft is attached to the spring shaft, and its thrust force is measured in axial direction. In the experiment, the amplitude of the voltages are constant ($A_E = 120$ V_{p-p}), and

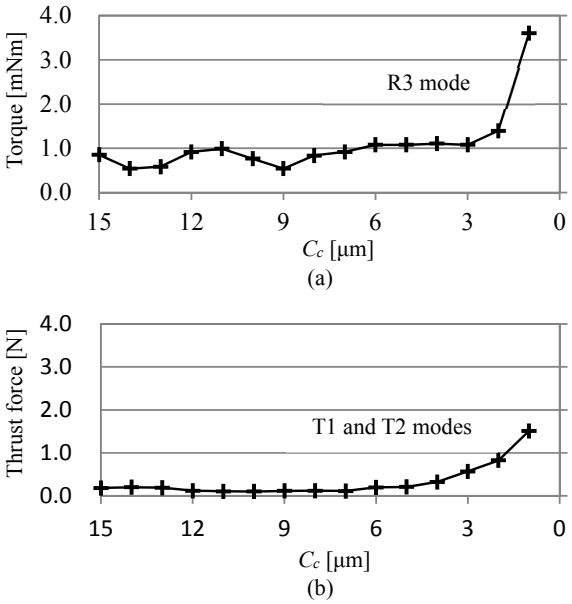

Fig. 12. Torque and thrust force in response to variations in the cylinder shaft diameter: (a) R3 and (b) T1 and T2 modes.

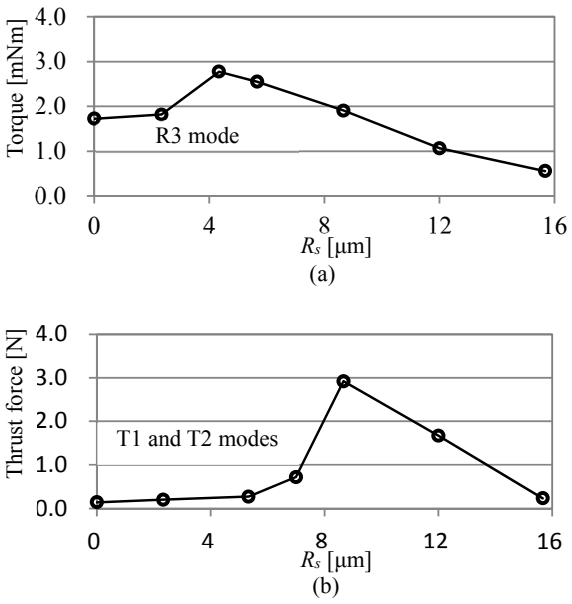

Fig. 13. Torque and thrust force in response to variations in the spring shaft diameter: (a) R3 and (b) T1 and T2 modes.

the frequency f_E is adjusted to make the torque and force maximum. After the voltages are applied, heat generation occurs. The stator and the shafts expand according to a coefficient of thermal expansion. Influence of the heat generation can be ignored in this experiment because the change of the clearance is very small. Incidentally, if the temperature rises by 5°C, The change of the clearance between the stator (coefficient of thermal expansion $\alpha = 17 - 18 \times 10^{-6}$ K^{-1}) and the shafts ($\alpha = 11 - 18 \times 10^{-6}$ K^{-1}) is less than 0.35 μm.

Figures 12(a) and **(b)** show the relation of the maximum torque and thrust force to the clearance C_c. When the clearance is minimum ($C_c = 1$ μm), both the torque and the thrust force peak ($T = 3.6$ mNm and $F = 1.5$ N). When there is no clearance ($C_c = 0$ μm), the motor cannot generate motions. It is due to that static friction is too large to drive the cylinder shaft.

Figures 13(a) and **(b)** show the relation of the maximum torque and thrust force to the reduction value R_s. The peak torque of $T = 2.8$ mNm and peak thrust force of $F = 2.9$ N are obtained at $R_s = 5$ μm and $R_s = 9$ μm), respectively.

We next discuss the difference in the peak thrust forces values between the cylinder shaft and the spring shaft (**Figs. 12(b)** and **13(b)**). It is seen that the peak thrust force of the spring shaft is roughly twice larger than that of the cylinder shaft. This is because the spring shaft can adjust the preload value precisely and optimally by changing its diameter. In other words, it is insufficient to optimize the preload by the cylinder shaft with 1 μm accuracy. Another interesting aspect is that the spring shaft has a difference between the torque peak and the thrust force peak: the torque peaks at $R_s = 5$ μm and the thrust force peaks at $R_s = 9$ μm (**Figs. 13(a)** and **(b)**). It is due to that the vibration amplitude of T1 and T2 modes is larger than that of R3 mode (**Fig. 6**). The motor can generate large thrust force with high vibration amplitude under the large preload, whereas a small preload with low vibration amplitude reduces the torque.

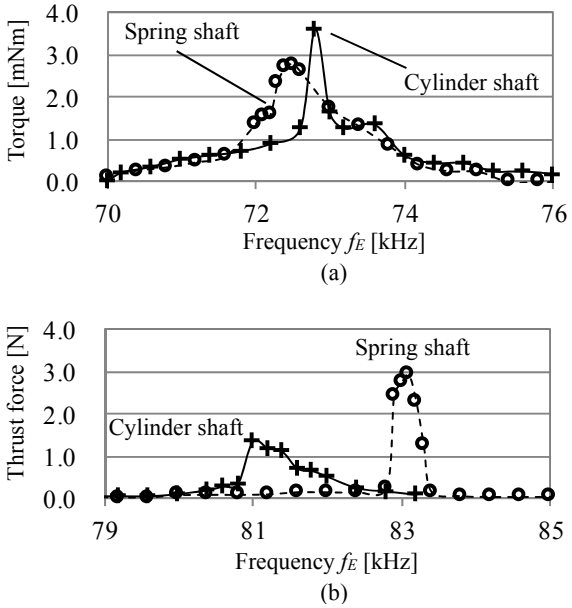

Fig. 14. Relationship of torque and thrust force to the frequency of applied voltages: (a) torque and (b) thrust force.

4.4. Frequency Characteristic Using the Optimal Diameters

Frequency characteristic of ultrasonic motors is important to be used for control of the torque and the thrust force. We examine the torque and thrust force of the rotary-linear ultrasonic motor by changing the frequency of the voltages at the constant amplitude $A_E = 120$ V$_{\mathrm{p-p}}$. **Fig. 14(a)** shows the behavior of the maximum torque when the frequency is changed. The torque peaks in the

neighborhood of the resonant frequency. The range of torque generation is 70–76 kHz in both the cylinder shaft and spring shaft. **Fig. 14(b)** shows the frequency characteristic of the maximum thrust force. The range of thrust force is 79–83 kHz in the cylinder shaft and is 81–85 kHz in the spring shaft. The thrust force of the spring shafts peaks slightly higher frequency than that of the cylinder shaft. The resulting torque and thrust force are non-linear with respect to the change in the frequency.

5. Conclusion

The torque and thrust force have been improved by optimizing the diameter of the cylinder and spring shafts experimentally. Compared to the previous rotary-linear ultrasonic motor with a similar sized stator and for the same applied voltages [9], the maximum torque of the spring shaft is 1.5 times larger and that of the spring shaft is 1.2 times larger; the maximum thrust force of the cylinder shaft is 4.4 times larger and that of the spring shaft is 8.5 times larger.

In the future, several design concepts for the realization of larger torque and thrust force will be explored, such as coating the output shafts with an appropriate material with an optimal friction coefficient. The proposed spring shaft works well at the optimal preload. Further, one of the advantages of the spring shaft application is its flexibility. Flexible robotics may be an interesting application of this motor.

Acknowledgements

This research has been supported in part by JSPS KAKENHI Grant Number 25709017 and the Leading Graduate School Program R03.

References:

[1] E. A. Mendrela and E. Gierczak, "Double-winding rotary-linear induction motor," IEEE Trans. on Energy Conversion, Vol.EC-2, pp. 47-54, 1987.
[2] S. Makino, T. Shikayama, I. Murokita, H. Yahara, and M. Ohto, "Direcet Drive θ-Z Motor for Rotary and Linear Motion," The Institute of Ekectrical Engineers of Japan, Vol.134, No.7, pp. 683-690, 2014.
[3] Koganei Corporation, http://ww1.koganei.co.jp/jp/ [accessed Dec. 22, 2015]
[4] N. Iwatsuki et al., "Precision positioning with a rotary-linear motor driven by a pair of 2-D ultrasonic actuators," in Micro Machine and Human Science, 1996., Proc. of the Seventh Int. Symposium, pp. 183-188, 1996.
[5] S. Sato et al., "Design of a precision rotary-linear dual-axis positioning system with a surface encoder," presented at the Proc. of SPIE, Int. Symposium on Optomechatronic Technologies (ISOT 2005) Sapporo, Japan, 2005.
[6] Y. Chen et al., "Study of a Mini-Ultrasonic Motor with Square Metal Bar and Piezoelectric Plate Hybrid " Japanese J. of Applied Physics, Vol.45, pp. 4780-4781, 2006.
[7] Y. Zhang, G. Liu, and J. Hesselbach, "On Development of a Rotary-Linear Actuator Using Piezoelectric Translators," IEEE/ASME Trans. on Mechatronics, Vol.11, No.5, pp. 647-650, 2006.
[8] S. Tuncdemir et al., "Design of Translation Rotary Ultrasonic Motor with Slanted Piezoelectric Ceramics," Japanese J. of Applied Physics, Vol.50, pp. 027301, 2011.
[9] T. Mashimo and S. Toyama, "Rotary-linear piezoelectric actuator using a single stator," IEEE Trans. on Ultrasonics, Ferroelectrics and Frequency Control, Vol.56, pp. 114-120, 2009.
[10] T. Mashimo and S. Toyama, "Rotary-Linear Piezoelectric Microactuator with a Cubic Stator of Side Length 3.5mm," IEEE Trans. Ultrasonics, Ferroelectrics and Frequency Control, 2010.
[11] T. Sashida and T. Kenjo, "Introduction to ultrasonic motors," New York: Oxford University Press, 1993.
[12] T. Mashimo and S. Toyama, "Vibration analysis of cubic rotary-linear piezoelectric actuator," IEEE Trans. on Ultrasonics, Ferroelectrics and Frequency Control, Vol.58, pp. 844-848, 2011.
[13] T. Funakubo et al., "Ultrasonic Linear Motor Using Multilayer Piezoelectric Actuators," Japanese Journal of Applied Physics. Pt. 1, Regular papers & short notes, Vol.34, pp. 2756-2759, 1995.
[14] T. Funakubo and Y. Tomikawa, "Characteristics of 10 mm Multilayer L1-F2 Mode Vibrator and Application to a Linear Motor," Japanese Journal of Applied Physics, Vol.42, pp. 3002-3006, 2003.
[15] K. Takemura and T. Maeno, "Design and control of an ultrasonic motor capable of generating multi-DOF motion," Mechatronics, IEEE/ASME Trans. on, Vol.6, pp. 499-506, 2001.
[16] M. Aoyagi et al., "A novel multi-degree-of-freedom thick-film ultrasonic motor," Ultrasonics, Ferroelectrics and Frequency Control, IEEE Trans. on, Vol.49, pp. 151-158, 2002.

Name:
Ayato Kanada

Affiliation:
Department of Mechanical Engineering, Toyohashi University of Technology

Address:
1-1 Hibarigaoka, Tempaku-cho, Toyohashi, Aichi 441-8580, Japan

Brief Biographical History:
2011- Toyohashi University of Technology

Name:
Tomoaki Mashimo

Affiliation:
Department of Mechanical Engineering, Toyohashi University of Technology

Address:
1-1 Hibarigaoka, Tempaku-cho, Toyohashi, Aichi 441-8580, Japan

Brief Biographical History:
2008 Ph.D. at Tokyo University of Agriculture and Technology
2008-2010 Robotics Engineer, Robotics Institute at Carnegie Mellon University
2011-2015 Assistant Professor, Toyohashi University of Technology
2016- Associate Professor, Toyohashi University of Technology

Main Works:
- "Micro Ultrasonic Motor using a One Cubic Millimeter Stator," Sensors and Actuators A: Physical, Vol.213, pp. 102-107, 2014.
- "Singularity-Based Four-Bar Linkage Mechanism for Impulsive Torque With High Energy Efficiency," ASME J. of Mechanisms and Robotics, Vol.7, No.3, 2015.
- "Experimental Verification of Elliptical Motion Model in Travelling Wave Ultrasonic Motors," IEEE/ASME Trans. on Mechatronics, Vol.20, No.6, pp. 2699-2707, 2015.

Membership in Academic Societies:
- Institute of Electrical and Electronics Engineer (IEEE)
- Japan Society of Mechanical Engineers (JSME)
- Japan Society for Precision Engineering (JSPE)
- Robotics Society of Japan (RSJ)

Name:
Kazuhiko Terashima

Affiliation:
Department of Mechanical Engineering, Toyohashi University of Technology

Address:
1-1 Hibarigaoka, Tempaku-cho, Toyohashi, Aichi 441-8580, Japan

Brief Biographical History:
1981 Ph.D. at Precision Mechanics of Kyoto University
1982-1983 Assistant Professor, Associate Professor at Toyohashi University of Technology
1991-1992 Visiting Researcher at Techinische Universitat Munchen
1994- Professor, Toyohashi University of Technology

Main Works:
• "Modeling and Optimal Control of a Rotary Crane Using the Straight Transfer Transformation Method," Control Engineering Practice, Vol.15, No.1, pp. 1179-1192, Jan. 2007.
• "Robust Liquid Container Transfer Control for Complete Sloshing Suppression," IEEE Trans. on Control Systems Technology, Vol.9, No.3, pp. 483-493, May 2001.
• "Development of Power-Assisted Wheelchair with H∞ Control to Maintain Robustness Against Load Uncertainly," Trans. of the Japan Society of Mechanical Engineers, Vol.74, No.738, C, pp. 152-160, 2008.

Membership in Academic Societies:
• Institute of Electrical and Electronics Engineer (IEEE)
• Society of Instrument and Control Engineers (SICE)
• Japan Society of Mechanical Engineers (JSME)
• Japan Foundry Engineering Society (JFS)